Estimation of semiconductor-like pigment concentrations in paint mixtures and their differentiation from paint layers using first-derivative reflectance spectra

Anuradha R. Pallipurath,[1a] Jonathan M. Skelton,[1b] Paola Ricciardi,[2] and Stephen R. Elliott[1]*

[1]*Department of Chemistry, University of Cambridge, Lensfield Road, Cambridge CB2 1EW, UK*

[2]*Fitzwilliam Museum, University of Cambridge, Trumpington Street, Cambridge CB2 1RB, UK*

[a]*Present address: School of Chemistry, University Road, National University of Ireland, Galway, Ireland*

[b]*Present address: Department of Chemistry, University of Bath, Claverton Down, Bath BA2 7AY, UK*

**To whom correspondence should be addressed: e-mail: sre1@cam.ac.uk; telephone: +44 (0)1223 336525*

ABSTRACT

Identification of the techniques employed by artists, e.g. mixing and layering of paints, if used together with information about their colour palette and style, can help to attribute works of art with more confidence. In this study, we show how the pigment composition in binary paint mixtures can be quantified using optical-reflectance spectroscopy, by analysis of the peak features corresponding to colour-transition edges in the first-derivative spectra. This technique is found to be more robust than a number of other spectral-analysis methods, which can suffer due to shifts in the transition edges in mixed paints compared to those observed in spectra of pure ones. Our method also provides a means of distinguishing paint mixtures from layering in some cases. The spectroscopy also shows the presence of multiple electronic transitions, accessible within a narrow energy range, to be a common feature of many coloured pigments, which electronic-structure calculations attribute to shallow band edges. We also demonstrate the successful application of the reflectance-analysis technique to painted areas on a selection of medieval illuminated manuscripts.

Keywords: fibre-optic reflectance spectroscopy, first-derivative analysis, function fitting, deconvolution, paint mixtures, electronic-structure calculations, vermillion, red lead, lead-tin yellow

Highlights

1. Artists use two common techniques to achieve different paint colour hues - mixing pigments in different fractions, and painting layers.
2. The pigment composition in a binary paint mixture can be reliably estimated by fitting the peak features in the first-derivative reflectance spectra, corresponding to the colour-transition edge in the reflectance spectra, to a sum of Gaussian functions, and analysing the resultant peak parameters.
3. The technique can also be used to distinguish between paint mixtures and painted layers in some cases.
4. The model coloured pigments in this study are found to have electronic structures featuring shallow band edges, leading to multiple transitions in a narrow energy range and hence to complex transition-edge features.

1. Introduction

Works of art have so far mostly been attributed to particular artists on the grounds of the artistic styles and colour palettes used. It is therefore important to understand the painting techniques used by artists on particular works under study. Artists used specific amounts of pigments to make paints with desired hues, and a painted layer could be a mixture of pigments or layers of one paint over another, producing wonderful optical effects to enchant their viewers. The proportions of pigments in a mixture, or the thickness of layers, can say much about an artist's technique. Having a precise knowledge of the working methods of an artist can aid in attribution, facilitate sympathetic restoration, and help to detect forgeries.

There is a growing need for techniques that allow analyses to be done onsite, and without having to remove samples from the artwork. Various non-invasive techniques, such as Raman [1-3], infra-red (IR) [4, 5] and X-ray fluorescence (XRF) [6] spectroscopies, and micro-X-ray diffraction (XRD) [5], have been used to identify the pigments, and in some cases even the binders [7-9], in paint films. Fibre-optic reflectance spectroscopy (FORS) in the visible and near-infrared range is another non-invasive method which is also robust in identifying pigments, and has shown promise in the identification of some paint binders [10-13]. Identification of pigments using techniques like FORS, XRF and Raman is in many ways, however, limited to identifying their presence, in the absence of stratigraphic information about the paint layers, as the spectra resulting from the absorption and scattering are invariably influenced by the surface texture of the paints, and possibly by complex layer structures consisting of paints, varnishes and/or support material, depending on the layer composition and thicknesses. A lot of effort is thus being made to obtain more stratigraphic information, non-invasively, where possible [4, 14, 15].

FORS has been analysed quantitatively using the Kubelka-Munk (KM) theory of diffuse reflectance, or the so-called “two-flux” model, an approach widely used to study materials as diverse as paints [16, 17], semiconductors [18], cosmetics on skin [19] and food [20, 21]. In their review, Berns *et al.* [22] give a comprehensive summary of the various implementations of the KM theory. The most commonly-used is the “paint approach”, where the spectrum of a paint mixture is modelled as a linear combination of the spectra of the pure components in the space of KM units. Dupis and Menu, in 2005, used these ideas to develop a method to identify the concentration of pigments in organic binding media [23]. It was later shown that KM theory could also be used to study paint mixtures [16]. Rodriguez and Fernandez (2005) further developed another interesting technique to characterise pigments in mixtures, using the second derivatives of reflectance spectra converted to KM units [24]. However, it has been reported that the usual solutions to the KM model did not yield satisfactory results in the identification of certain red pigments [16].

Various other techniques based on the derivatives of reflectance spectra have also been used for characterisation. Indeed, there exists an entire field of “derivative spectroscopy” [25-28] dedicated to the use of derivatives to extract maximum information from spectra. The most commonly-employed quantities are the heights of peaks in first- [16, 29] or second-derivative spectra [24], which allow features in the reflectance spectra to be more easily identified, in part by discarding unwanted features such as a constant baseline shift. For example, first-derivative spectra have been used as a means to overcome spectral differences observed due to particle size and surface roughness [16]. The use of second and higher derivatives is often less preferable, however, due to the artefacts that may be present in such signals [26].

In the present work, we develop a procedure to deconvolute the peak features in the first derivatives of FORS spectra, corresponding to the colour-transition edges in the reflectance spectra, and show how the ratio of the areas under the characteristic peaks ascribed to different pigments can

be used to quantify the composition of binary paint mixtures. This analysis of first-derivative spectra can also in some cases allow FORS data to be used to differentiate between pigment mixtures and paint layers. We also find that certain pigment mixtures lead to quantifiable blue shifts in the transition edges, which can be problematic for other analysis methods such as the "paint approach" variant of KM theory. As a proof of concept, we demonstrate the application of our method to the characterisation of red painted areas on two medieval illuminated leaves from the collection of the Fitzwilliam Museum, Cambridge, *viz.* MS McClean 79 (Book of Hours, Paris, c. 1405-1410; folios 11r and 71r) and MS 62 (Book of Hours, Northern France, probably Angers, c. 1431; folio 18v)[30]. Finally, we employ electronic-structure calculations to investigate the origin of the complex structure of the colour-transition edges in three commonly-used coloured pigments, which appears to be a consistent feature of these systems.

Finally, we employ electronic-structure calculations to investigate the origin of the complex structure of the colour-transition edges in three commonly-used coloured pigments pigments, which appears to be a consistent feature of these systems.

2. Experimental

Sample preparation

All the pigments used in this study were purchased from Kremer Pigments, Inc. and used without any further processing. The grain sizes of the pigments as supplied were not specified. Gum arabic resin (Kordofan Grade) was imported from the Middle East via L. Cornelissen and Son, London, and the binder was prepared by dissolving the resin in water.

We considered paint mixtures containing three yellow and red pigments commonly used in medieval artwork, *viz.* lead-tin yellow (Pb_2SnO_4; LTY), red lead (Pb_3O_4; RL) and vermillion (α-HgS; VRM), as well as tints of LTY and RL with the white pigment, basic lead white ($2Pb_2CO_3$. $Pb(OH)_2$; LW). Paint films were made up in one of two ways: binary mixtures of LW/RL, LW/LTY, RL/LTY and RL/VRM were made with various pigment mass ratios (2:1, 3:2, 1:1, 2:3, 1:2), and we also made samples formed of superposed layers of pure paints of RL and LTY, and RL and VRM. For the latter, the thicknesses of the layers were not controlled, as is the case in real artwork samples.

The binder was prepared by dissolving gum Arabic in water until a suitable gum-like consistency was obtained, after which the concentration of the gum in water was kept fixed while preparing the paint samples. To prepare the paint mixtures, the two pigments (wt/wt) were first geometrically mixed, and a few drops of the binder added to obtain a paint of a consistent thickness. The paints were then brushed on to microscope glass slides and allowed to dry on the bench. To prepare the layered samples, paints of the pure pigments were prepared in a similar fashion to the mixtures, and the first layer painted onto a glass slide and allowed to dry for an hour before application of a second layer. One of each sample were prepared, but with a sufficiently large surface area that reflectance spectra could be recorded from multiple spots.

We note that these methods were chosen to mimic the techniques used by medieval artists as closely as possible, in line with the focus of this study on applications to conservation science.

Spectroscopy and data processing

Reflectance spectra were obtained using a FieldSpec 4 spectroradiometer (ASD Inc., USA), in the wavelength range of 350-2500 nm at a spectral resolution of 3 nm at 700 nm, and 10 nm at 1400 nm and 2100 nm. Before acquiring spectra, the instrument was calibrated using a 99% reflective spectralon standard (Labsphere). A minimum of three spectra were recorded from each paint sample, taken randomly from different spots on the film. We note that we did not attempt to collect spectra at a consistent working geometry; although the FieldSpec 4 has a suitable "contact-probe" accessory for doing so, it is not generally possible to use such a device to analyse cultural-heritage objects (including the manuscripts analysed in the present study) due to the risk of surface damage, and so we opted not to use it when collecting data from the model paint films, in order to emulate the same issues as would be present when analysing artwork samples.

The reflectance spectra were then differentiated using a seven-point finite-difference stencil. The 350-750 nm colour-transition regions of the resulting derivative spectra were modelled as a sum of Gaussian peak functions, i.e.:

$$R'(\lambda) = \sum_n \frac{A_n}{\sqrt{2\pi}\sigma_n} \exp\left[-\frac{(\lambda - \mu_n)^2}{2\sigma_n^2}\right] \quad (1)$$

where λ is the wavelength and the sum runs over n peak functions with area A, central wavelength μ and bandwidth σ. The bandwidth is related to the full-width at half-maximum (FWHM) of the peak profile according to:

$$\mathrm{FWHM} = 2\sqrt{2\ln 2}\,\sigma \quad (2)$$

The fitting procedure was implemented in the Python [31] programming language, using the Numpy [32] and SciPy [33] packages. For function fitting, we used the "minimize" routine available in SciPy 0.14.0, which implements the bounded L-BFGS-B algorithm.[34, 35] We used the root-mean-square difference between the measured and fitted derivative spectra as the objective function to be minimised, and constrained the area and bandwidth to be ≥ 0. The parameters A_n, μ_n and σ_n for the spectra of the pure components were fitted by eye and refined using the minimisation algorithm. Appropriate combinations of the optimised parameters for the pure paints were then used as the initial parameters for fitting the spectra of the mixtures and glazes.

The quality of the fits was verified by integrating the fitted derivative spectra to reconstruct simulated colour-transition edges. The arbitrary constant of integration - corresponding to a constant baseline shift in the measured reflectance spectra, which is effectively discarded during differentiation - was determined as the average difference between the fitted and simulated reflectance spectra across the fitted 350-750 nm range.

To perform a basic comparison of our approach to KM theory, we considered the most basic "paint-approach" variant of the theory. In this implementation, the relation between the absorbance of, and scattering from, a material is given by [29]:

$$\frac{K(\lambda)}{S(\lambda)} = \frac{(1 - R(\lambda))^2}{2R(\lambda)} \quad (3)$$

where K and S are the absorption and scattering coefficients, defined as the cross-sectional area per unit volume of the medium that absorbs and scatters, respectively, and R is the reflectance. In the paint approach, the spectrum of a paint mixture, in K/S units, is assumed to be a linear combination of the spectra of the two pure components in a given ratio, i.e.

$$\left(\frac{K}{S}\right)_{mix} = \left[\frac{c_1}{c_1 + c_2}\left(\frac{K}{S}\right)_1 + \frac{c_2}{c_1 + c_2}\left(\frac{K}{S}\right)_2\right] \quad (4)$$

Since we found our fitted spectra to provide a quantitative reconstruction of the transition-edge features in the original spectra (see results and discussion), we opted to utilise the procedure as a pre-processing step to "denoise" the spectra before analysis.

Spectra of pure paints were fitted as described above, and smooth transition edges obtained by numerically integrating the summed peak functions (**Eq. 1**) over the transition-edge region. The spectra were then normalised to a saturation value of unity, and converted to K/S units using **Eq. 3**. We then compared K/S spectra obtained directly from the integrated fits of the paint-mixture spectra to the corresponding simulated ones using **Eq. 4**.

Electronic-structure calculations

During our analysis, we observed that all three coloured pigments displayed complex colour-transition edges with multiple features. To investigate the microscopic origin of this phenomenon, we carried out electronic-structure calculations on tetragonal Pb_3O_4 (RL), α-HgS (VRM) and $SnPb_2O_4$ (LTY), using the published crystal structures [36-38] as a starting point. Full technical details of these calculations may be found in the **supporting information**.

3. Results and discussion

Spectra analysis

Fig. 1 illustrates the results of our fitting procedure applied to spectra of pure RL, pure LTY and a 50:50 wt/wt mixture of the two. As shown, the prominent colour-transition edges in the 350-750 nm region of the spectra correspond to peaks in the derivative spectra, which we found were very well modelled as a sum of Gaussian functions (see **Eq. 1**), a confirmation of which is provided by the numerical integrals of the fitted functions, yielding an excellent reproduction of the measured transition edges.

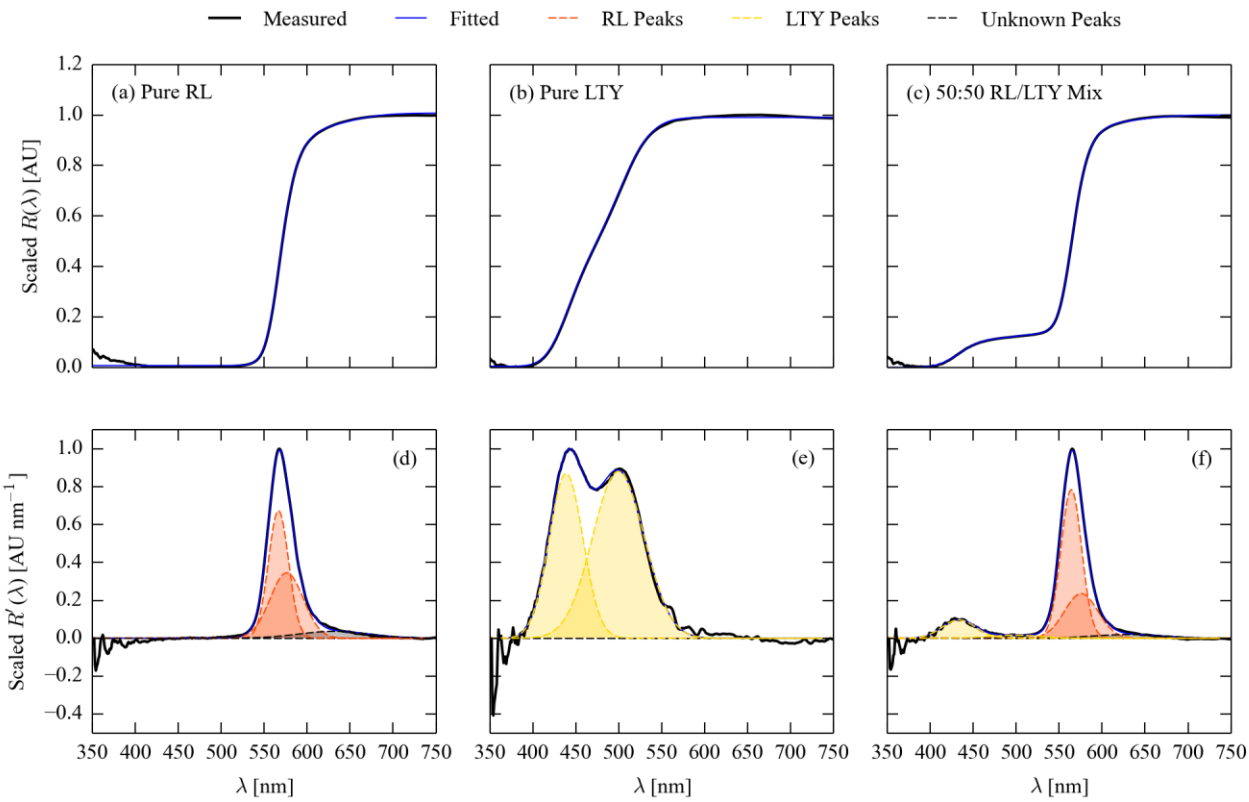

Figure 1 Illustration of the first-derivative fitting analysis procedure applied to spectra of paints made up with pure red lead (a, d), pure lead-tin yellow (b, e) and a 50:50 wt/wt mix of the two (c, f). The colour-transition regions of the reflectance spectra (a - c) are differentiated to obtain derivative spectra (d - f). The transition edges in the former correspond to peaks in the derivative spectra, which are well fitted by a sum of Gaussian peak functions. The individual fitted peaks and the sum are superimposed on the measured derivative spectra in (d - f). Integrating the fitted functions yields a very good reproduction of the edge features in the original spectrum, as illustrated by the close match between the measured reflectance spectra and superimposed numerical integrals of the fitted derivative spectra in (a - c).

We found that the derivative spectra of the three pure paints considered in this work could be fitted by two Gaussian functions. The wavelength and full-width at half-maximum (FWHMs) of these characteristic peaks are given in **Table 1**. For LTY, the colour transition is clearly a composite feature composed of two distinct edges (**Figs. 1 (b, e)**), corresponding to two peaks with a 3:5 area ratio in the derivative spectrum. The spectra of pure RL (**Figs. 1 (a, d)**) and VRM (see **supporting information Fig. S7**) are likewise well fitted by a pair of Gaussian functions, although in these pigments the central wavelengths of the features are much closer, and the presence of the two components in the transition edge is less easily discerned. Furthermore, the derivative spectra of both red paints also appear to contain a broad third feature centred above 600 nm, whereas this was consistently absent in the LTY spectra; the origin of this additional peak is unclear, but may be due to an interaction between the red pigments and the paint binder. A complete set of representative reflectance and derivative spectra of the paint samples prepared in this study, together with the fits, is presented in the **supporting information (Figs. S5-S25)**.

Pigment	Peak 1		Peak 2		Area Ratio
	μ [nm]	FWHM [nm]	μ [nm]	FWHM [nm]	
Lead-tin yellow	438.78 ± 0.19	46.56 ± 0.61	500.34 ± 0.66	72.34 ± 1.34	0.63 ± 0.02
Red lead	566.63 ± 0.01	27.35 ± 0.50	576.27 ± 0.19	45.48 ± 0.10	0.79 ± 0.04
Vermillion	596.35 ± 0.03	53.29 ± 0.01	601.45 ± 0.09	24.87 ± 0.01	1.66 ± 0.02

Table 1 Characteristic peaks in the derivative-reflectance spectra of pure lead-tin yellow (LTY), red lead (RL) and vermillion (VRM) paints. The table lists the central position, μ, and full-width at half-maximum (FWHM) of the two peak functions, together with the ratio of the areas of the first and second peaks. The errors are given as $\pm$ 1 standard deviation of the average over the three different spectra taken from each sample.

We were able to obtain satisfactory fits of our model paint mixture and glaze samples by fitting to a sum of the peaks observed in the spectra of the pure paints (e.g. **Fig. 1 (f)**), including only one peak for the unassigned component observed in the spectra of paints with red pigments. To ascertain whether it might be possible to extract compositional information about a binary mixture from these fits, we analysed a series of paints made up of mixtures of RL and VRM in various mass ratios, *viz*. 2:1, 3:2, 1:1, 2:3 and 1:2, corresponding, respectively, to 66.7, 60, 50, 40 and 33.3 % RL by mass (**Fig. 2**). These ratios were chosen instead of the more usual 5, 10 and 15 % additions of one component to the other in order to obtain a calibration plot covering the central range of the mixtures of RL and VRM that could in principle occur in actual paints.

In contrast to the RL/LTY system, where the much stronger absorption of RL leads to more prominent features from this pigment in the derivative spectra (**Fig. 1 (c, f)**; see also **Fig. S1** in the supporting information), VRM and RL show a comparable absorption. The transition-edge region of RL/VRM mixtures shows two prominent maxima, each of which can be attributed primarily to each pigment. As the mass proportion of RL in the mixture increases, the shorter-wavelength feature grows while the longer-wavelength one diminishes, and vice versa (**Fig. 2 (b)**). On closer examination, there is also some fine structure between the two maxima, which was clearest in the spectra of the 1:1 mixture, but was not always discernible.

Our fitting procedure effectively allows the relative contribution of features from the two pigments to the overall transition-edge feature to be separated. For the RL and VRM mixtures, the contribution to the total area under the combined feature in the derivative spectrum shows a good linear correlation with the mass ratios in which the pigments were combined (**Fig. 2 (c)**), allowing a calibration curve to be constructed which could be used to estimate quantitatively the composition of an unknown paint mixture. For this analysis, we averaged the area ratios obtained from analysis of the multiple spectra recorded from each paint sample, and included error bars on the plot by calculating the standard deviation; this gives some idea of the variability in the area ratios, which we found were generally quite small.

Another noteworthy observation which can be made from **Fig. 2 (b)** is that the RL features in the derivative spectra appear to undergo a blue shift with increasing VRM composition - from our fitting, we estimate shifts of 6.3 nm and 0.9 nm for the major and minor peaks, respectively, between the pure RL and the mixture with 66.7 % VRM. The former is significantly outside the estimated error on the position of this peak in the single-component paint. We note that this peak shifting would make the use of simpler methods for quantifying the composition, such as the relative intensities at fixed wavelengths, less reliable than the present fitting technique.

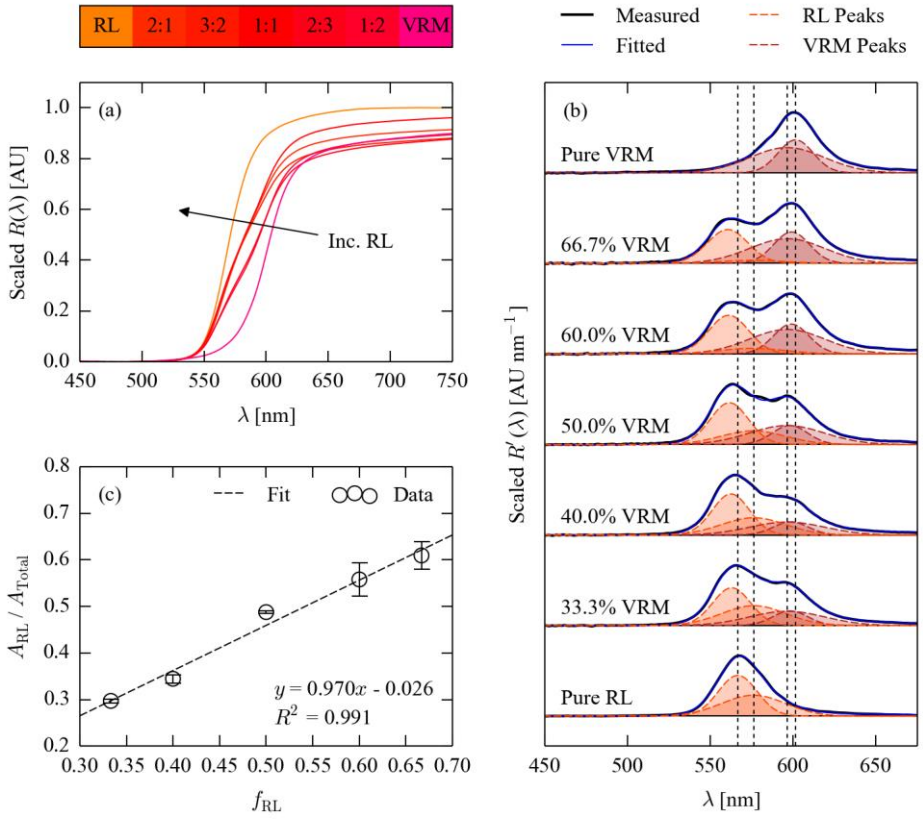

Figure 2 Comparison of the reflectance (a) and derivative (b) spectra of a series of paint mixtures containing red lead (RL) and vermillion (VRM) in different mass proportions. The relative contribution of features from the two pigments to the area under the composite transition-edge feature follows a linear trend with the mass composition (c), which could be used to estimate quantitatively the pigment composition of an unknown paint. The additional long-wavelength peak used to fit the derivative spectra (see text) is not shown in (b). The markers in (c) show the average ratios from fitting spectra recorded from multiple points on the various paint films, and the error bars show $\pm$ 1 standard deviation.

A similar analysis carried out on mixtures of LTY and RL (**Fig. S1**) showed a similar systematic variation in the spectra with mass composition, and the relative areas could again be fitted reasonably well to a linear trend to obtain a calibration curve. In contrast to the trend in **Fig. 2**, however, the weaker absorption of LTY meant that the LTY peaks contributed < 25 % of the total area under the composite feature even when present in a majority 66.7 % by mass. As a result, whereas one might anticipate from **Fig. 2** that the calibration curve for the RL/VRM system might remain linear over the complete range of compositions between the endpoints, non-linear behaviour would be expected towards the LTY end of the RL/LTY system. Finally, as with the RL/VRM system, we again observed significant blue shifting of both the RL and LTY features in the mixtures with respect to the pure compounds, with a maximum shift of 5.7 and 3.7 nm for the two LTY and RL features, respectively.

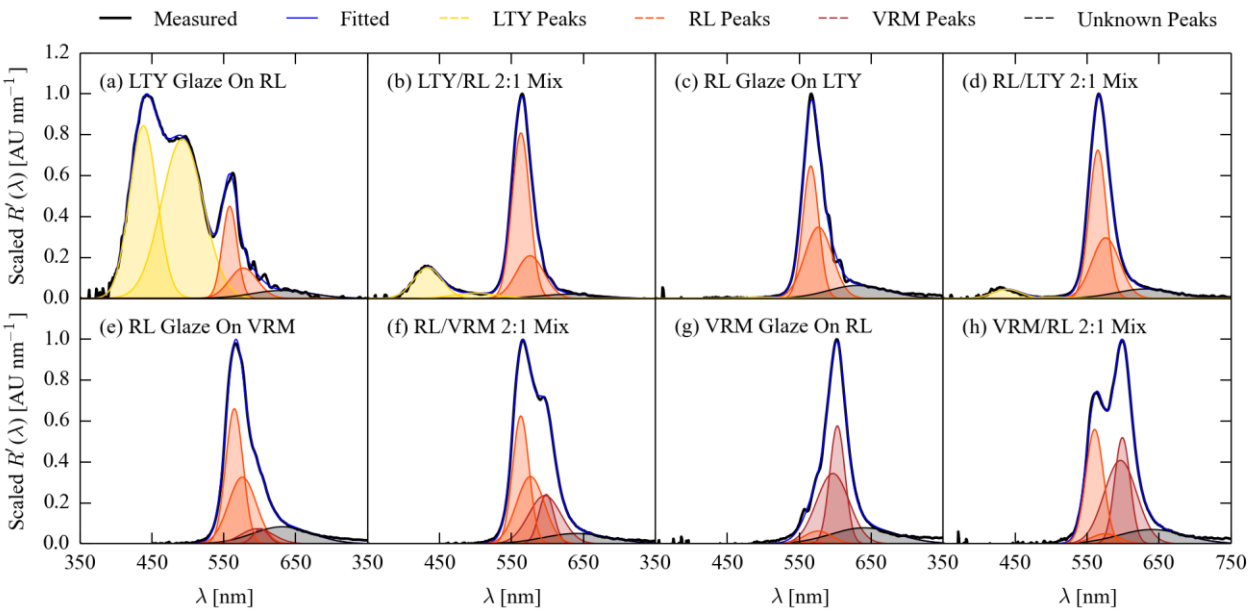

Figure 3 Comparison of first-derivative reflectance spectra of two-component layers (i.e. glazes of one pure paint on another) and mixtures of the two paints. Plots (a) and (b) compare the spectra of a lead-tin yellow (LTY) glaze on a red lead (RL) layer with a paint mixture made up with the pigments in a 2:1 weight ratio, while plots (c) and (d) compare the opposite cases of a RL glaze on an LTY layer and a RL-rich mixture. Plots (e) and (f) show the spectra of an RL glaze on a layer of vermillion (VRM) and a RL/VRM 2:1 mixture, while the spectra in (g) and (h) show the corresponding VRM-rich mixture.

FORS is a surface technique, so in a layered paint film the recorded spectrum would be dominated by features from the top layer. However, depending on the layer thickness, and the optical properties of the pigments in the top layer and underlayer(s), it may also be possible to observe spectral features from the latter. In the present study, we observed that an analysis of the derivative reflectance spectra could indeed in some cases allow paint layers (glazes) to be distinguished from homogenous mixtures.

Fig. 3 compares representative derivative spectra of glazes of LTY on RL, RL on LTY, RL on VRM and VRM on RL with the corresponding paints made up in a 2:1 mass ratio with the top-layer pigment as the major component. In the spectrum of the LTY glaze on RL, prominent features from the underlayer are visible in the spectrum, although the LTY features are far more prominent than in the derivative spectrum of the 2:1 LTY/RL mixture. On the other hand, a RL glaze on LTY completely masks the spectral features of the latter, which remain visible, albeit weakly so, in the spectrum of the RL-rich mixture. This can be explained naturally by the much more intense absorption of RL in comparison to LTY, which is clearly evident in the spectra of the 1:1 mixture in **Figs. 1 (c, f)** and those of the RL/LTY mixtures in **Figs. 3 (b, d)**, where the RL features are invariably much more prominent than the LTY ones. On the other hand, as seen in the data in **Fig. 2**, the red pigments RL and VRM are approximately equal in their absorption intensity. In the glazes with these pigments, the features from the underlayer are instead visible as shoulders on prominent features from the top layers, as opposed to clear peaks in the mixtures.

In the present study, we did not control the layer thicknesses in our model glazes, and so we simply note that inspection of the derivative spectra, with reference to spectra of suitable model samples, might be used to identify layering and to distinguish it from mixing, in cases where the underlayer is made up of a pigment which shows comparable or stronger absorption than the top layer. However, in a similar manner to the mixtures, we would expect the area proportions under the top- and lower-layer features to correlate to the layer thickness, and hence this technique might provide a non-invasive means of obtaining quantitative stratigraphic information in some cases. We leave a more detailed exploration of this possibility to a future study.

Finally, we also considered tints of LTY and RL with LW (**Figs. S2 and S3**, respectively), which similarly showed interesting trends. Being white, LW has no features in the colour-transition region, and thus, as might be expected, the only features visible in the derivative spectra are from the coloured components. However, like in the case of RL/VRM mixtures, the RL features in the first derivative spectra blue shift with increasing LW content. In addition to the apparent blue shift, there is also a change in the ratio of the areas under the two RL features, with the major peak at ~566 nm gaining more prominence at the expense of the minor one at ~576 nm as the LW content increases. With LTY, on the other hand, we observed no significant blue shift with LW content, but noted a similar change in the ratio of the area under the two prominent LTY peaks, with the transition edge at ~500 nm becoming more prominent with respect to the shorter-wavelength feature at ~439 nm with increasing amounts of LW.

In principle, a change in the prominence of one transition edge feature with respect to another may be indicative of changes in the chemical environment and/or electronic structure of the pigment, but the mechanisms which might lead to this are not well understood, and more detailed studies need to be carried out into the effects of a number of potential variables including the binding medium, the pigment used to tint, and the pigment particle size. Nonetheless, this analysis does suggest that an analysis of derivative reflectance spectra may also be used to characterise tints, perhaps in conjunction with other techniques to identify their use in the first instance.

Comparison to Kubelka-Munk analysis using the "paint approach"

An interesting observation extracted from our analysis of the paint mixtures is that mixing pigments can produce systematic blue shifts in the transition-edge features of one or both components, depending on the system.

Since the composite transition edge in such mixtures is then not a simple linear combination of those of the pure components, this behaviour is likely to be problematic for the simpler paint approach to KM analysis [29]. To test this, we took reflectance spectra of RL and VRM, pre-processed using our fitting procedure to obtain smooth transition edges (see **Experimental**), converted them to the KM units of K/S using **Eq. 3**, and then compared K/S spectra of three RL/VRM mixed paints simulated using **Eq. 4** to those obtained from the actual spectra (**Fig. 4**).

Considering a model colour transition, where the reflectance goes from zero below the edge to unity above it, according to **Eq. 4** the K/S function will approach the edge from infinity (i.e. below the edge, the absorption is much larger than the scattering coefficient, $K \gg S$), and will fall to zero above it (corresponding to a regime where the paint film only displays scattering, i.e. $S \gg K$). For RL and VRM, the transition edges show substantial overlap, and the main differences in the K/S spectra occur over a window of ~100 nm (**Figs. 4 (a, b)**).

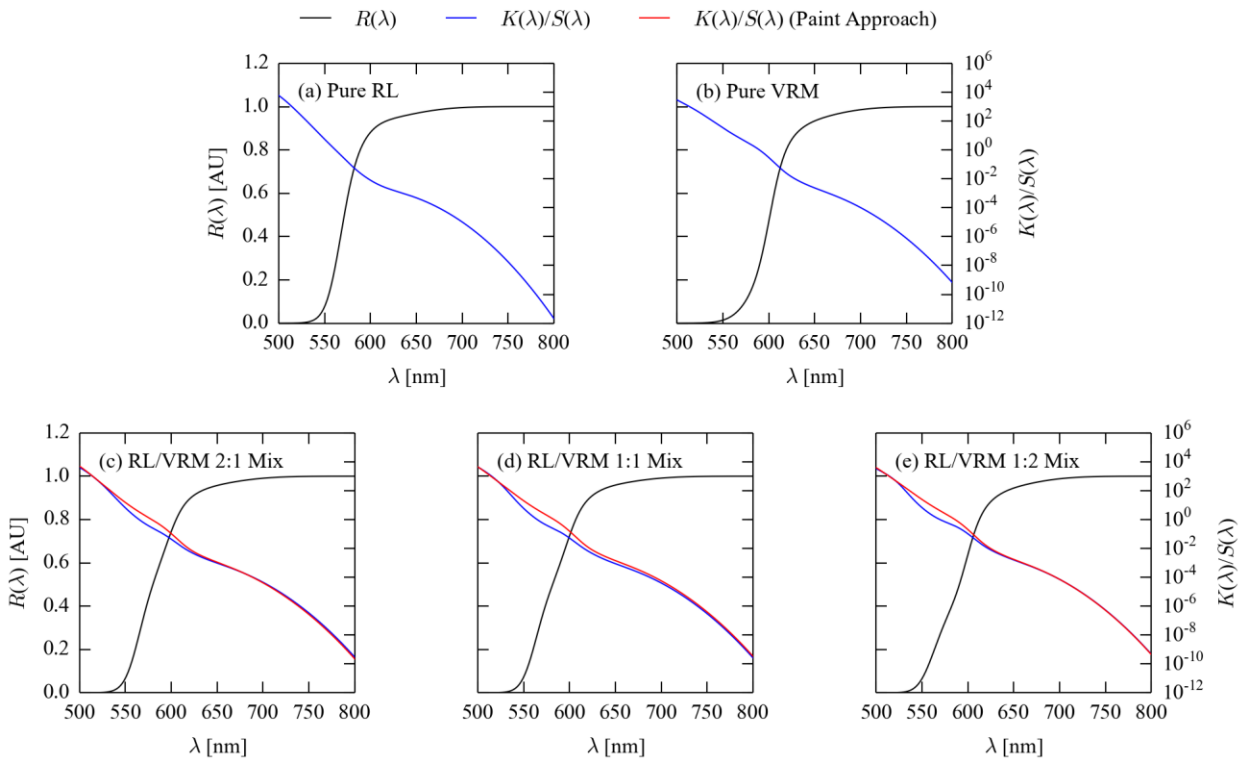

Figure 4 Modelling the spectra of paint mixtures of red lead (RL) and vermillion (VRM) using the "paint approach" to Kubelka-Munk (KM) theory. Plots (a) and (b) show the reflectance spectra (black) of pure RL and VRM paints, respectively, normalised to the range [0, 1] and converted to the KM units of K/S (blue), where K and S are the absorption and scattering coefficients, respectively (see **Eq. 3**). Note that the K/S functions are plotted on a logarithmic scale. Plots (c - e) show the reflectance and K/S spectra of RL/VRM paint mixtures made up with different mass proportions of the pigments, together with the simulated K/S spectra (red) obtained by combining the spectra of the pure components in the same ratios according to **Eq. 4**.

The $1/2R$ term in the expression for K/S (**Eq. 3**) makes this function highly sensitive to subtle changes in the form of the edge, which is quite clearly evident from a comparison of the K/S spectra of the three RL/VRM mixtures simulated using **Eq. 4** to the spectra obtained for the actual edges (**Figs. 4 (c - e)**). The deviation is larger in the 1:1 mixture than in the 2:1 mixtures, presumably because the spectrum of this mixture differs most strongly from that of either of the pure components. This analysis thus confirms that the blue shifting observed in some mixed paints can indeed potentially cause issues for this simple formulation of KM theory.

Interestingly, a similar analysis of our RL/LTY mixtures using the same approach (**Fig. S4**) revealed another clear shortfall of this technique. In contrast to the case of the RL/VRM system, the transition edges of RL and LTY are well separated in wavelength, such that the K/S function of the former is approaching infinity where that of LTY contains the fine structure from the transition edge. As a result, the paint approach predicts that the strong absorption of RL should more or less completely mask the LTY transition edge. While the spectra in e.g. **Figs. 1 (c, f), 3 (b) and S1** show that the transition-edge features of RL are much more prominent than those of LTY over a range of mixing proportions, the LTY features are not as strongly masked as this KM analysis would suggest.

This implies that the paint approach is likely to be ill-suited to systems where the colour transitions of the components are spectrally well separated, which may be a reason why previous studies using the model have proven to be challenging [16].

We must note, however, that there are more sophisticated solutions to the KM model for different systems, and improvements to the model have been made since it was first proposed [39, 40]. The main limitation in the context of artwork analysis is that more accurate solutions, e.g. the Hapke model [41], require additional parameters, such as the grazing angle and sample layer thicknesses to be known. This is generally not feasible when carrying out artwork analysis, as the nature of the samples can make it difficult to maintain the light source and detector at fixed angles while still acquiring meaningful data from areas of interest, and stratigraphic information is typically not available.

Application to the characterisation of red painted areas in medieval manuscripts

Finally, we have successfully demonstrated the application of our technique for conservation science by using it to characterise red painted areas in two medieval manuscripts from the collection of the Fitzwilliam Museum, Cambridge, *viz.* MS McClean 79 and MS 62.

Fig. 5 (a) shows one of the samples analysed (MS McClean 79, folio 71r), which contains a large red painted area. On fitting a derivative reflectance spectrum recorded from this area using our technique (**Fig. 5 (b)**), we obtained peaks close to those characteristic of RL and VRM, with the fitted spectrum having an appearance similar to one of the RL/VRM mixtures in **Fig. 2 (b)**. Using the calibration plot in **Fig. 2 (c)**, we estimated the mixture to have ~45 % RL content. However, a visual inspection by a trained eye gives more of an impression of an RL underlayer with a very thin layer of VRM (i.e. a highlight). To better understand this conundrum, a more detailed study of paint glazes with controlled layer thicknesses would be required, which we defer to a future study.

	Peak Positions [nm]				
Manuscript	**1**	**2**	**3**	**4**	**Tentative Assignment**
MS McClean 79 (f71r)	564.46	575.43	596.44	596.89	RL/VRM mixture (approx. 45.0% RL) [XRF/FT-Raman suggest alternative red pigment]
MS McClean 79 (f11r)	566.61	576.16	600.98	606.67	VRM with possible RL underlayer
MS 62 (f18v)	566.27	576.59	596.38	598.71	RL/VRM mixture (approx. 44.2% RL)
	563.47	572.77	606.07	611.86	RL with possible VRM underlayer
	567.34		603.22	610.60	VRM with possible RL underlayer

Table 2 Positions of the fitted peaks in the five derivative reflectance spectra in **Figs. 5 (b-f),** along with tentative assignments.

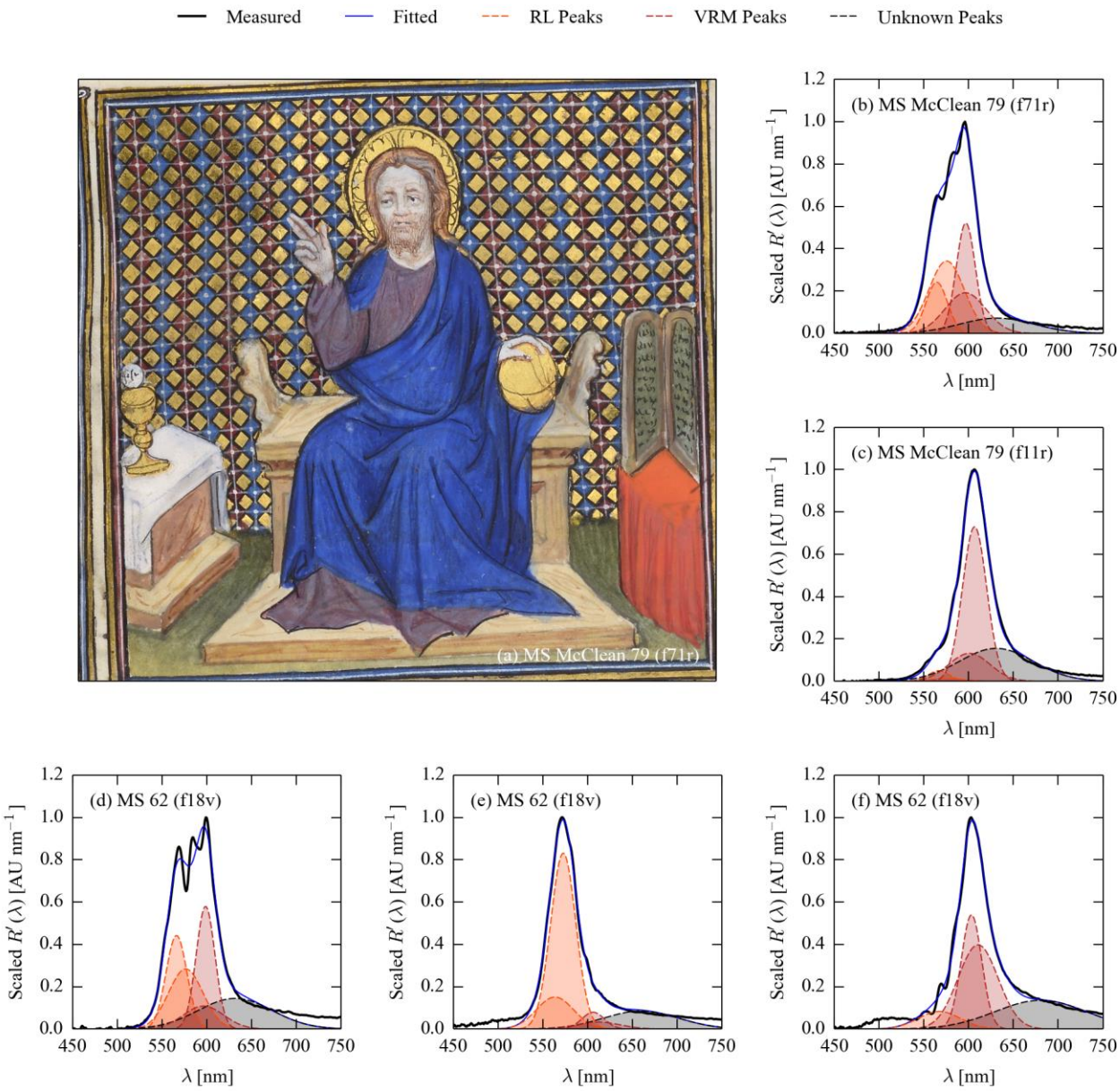

Figure 5 Application of the derivative-reflectance spectrum analysis technique to painted areas on illuminated medieval manuscripts. Panel (a) shows a detail of folio 71r of one of the two manuscripts studied, MS McClean 79, with a large red painted area (image reproduced with permission from the Fitzwilliam Museum, Cambridge). Plot (b) shows the colour-transition region of a derivative spectrum of this area, modelled as a sum of Gaussian functions corresponding to the characteristic peaks in red lead (RL) and vermillion (VRM). Plot (c) shows a similar analysis of the derivative spectrum of a red spot from another folio of MS McClean 79 (11r), while plots (d - f) show spectra taken from folio 18v of another manuscript, MS 62. The spectra in (b) and (d) can be tentatively assigned as mixtures of RL and VRM in roughly equal proportions (using the calibration plot in **Fig. 2 (c)**), while the spectra in (c)/(f) and (e) can be assigned as VRM glazes on RL and RL glazes on VRM, respectively.

Fig. 5 (c) shows a derivative spectrum recorded from another folio of MS McClean 79 (11r), and **Figs. 5 (d - f)** show spectra recorded from three different red areas on folio 18v of MS 62. As for the spectrum in **Fig. 5 (c)**, and for our analysis of the RL/VRM mixtures and glazes, all four spectra were fitted to the characteristic RL and VRM peaks, plus a single unknown peak centred above 600 nm. The fitted peak positions are listed in **Table 2**, together with tentative assignments.

The spectrum from MS McClean 79 folio 11r (**Fig. 5 (c)**) could be straightforwardly assigned as a layer of VRM on RL due to the dominant contribution of peaks at the characteristic VRM positions to the fitted spectrum, together with a shoulder from peaks at the RL wavelengths. Of the three red areas in folio 18v from MS 62, the red used to paint St. Mark's robe (**Fig. 5 (d)**) was assigned as a RL/VRM mixture with 44.2% RL, while the red robe of a side miniature and a coat of arms (**Figs. 5 (e) and (f)**, respectively) were assigned as layers of RL on VRM and VRM on RL, respectively.

It is worth noting that the painted areas on cultural heritage objects can, in general, be expected to be more complex substrates than the model paint films analysed in this work. In particular, the possible use of different binding media from the gum arabic analysed in this work, and of more complex (e.g. ternary) pigment mixtures, together with possible reflectance features from other components such as varnishes, could all make unambiguous assignment of paint compositions less clear cut than in our model studies.

An added problem while analysing illuminated manuscripts is the relatively small area of analysis, making details and highly reflective gilding in the surrounding areas contribute to the reflections being analysed. Hence, care must be taken during the analysis of such areas and the results should be compared to other techniques such as XRF. As a case in point, any or all of these could account for the unfitted fine structure in the spectra in **Figs. 5 (b, d, f)**. On the other hand, future systematic studies of these variables, and the complementary use of other, non-invasive, techniques such as FT-Raman to identify other components and hence select suitable references, could render the present technique a valuable tool in conservation science.

Electronic-structure calculations

To better understand the origin of the multiple transition edges in the reflectance spectra of RL, VRM and LTY, we performed density-functional theory (DFT) calculations to investigate the electronic structures of the three pigments (see **supporting information** for details). **Fig. 6** shows electronic band dispersions and density of states (DoS) curves calculated at the GGA (PBEsol) level of theory, together with images of the optimised structures. The optimised lattice parameters are listed in **Table S1**, and the smallest direct and indirect bandgaps computed from the band dispersions and DoS meshes are collected in **Table 3**.

The calculated gaps indicate all three pigments to be indirect-gap semiconductors, although in each case the direct gap is very close to the indirect one. Another shared feature is that the valence bands of all three systems possess flat regions (i.e. segments with small band dispersion), which would in principle give rise to a number of indirect transitions with similar energies. The gaps fall into the order RL ~ VRM < LTY, and thus correctly predict a blue shift in the transition edge of the yellow pigment compared to the red ones, but the PBEsol gaps are substantially underestimated.

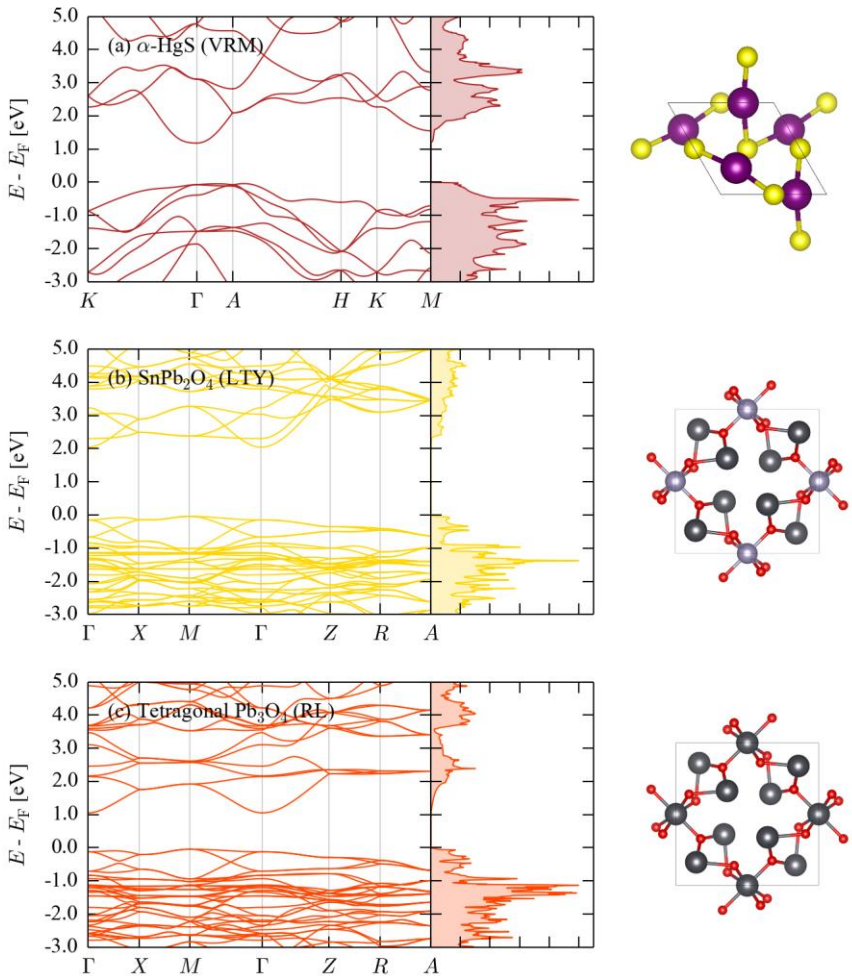

Figure 6 Electronic band dispersions and density of states curves calculated for α-HgS (VRM; a), $SnPb_2O_4$ (LTY; b) and tetragonal Pb_3O_4 (RL; c) structures at the PBEsol (GGA) level of theory.[42] Images of the optimised structures, taken along the *c* axis (i.e. through the *ab* plane) are shown alongside the plots. The colour coding of the atoms is as follows: O - red, S - yellow, Sn - steel blue, Pb - dark grey, Hg - violet. These images were generated with the VESTA software.[43]

	$E_{g,PBEsol}$ / eV					
	Band Dispersion		DoS Mesh		$E_{g,HSE06}$ / eV	
System	$E_{g,dir}$	$E_{g,indir}$	$E_{g,dir}$	$E_{g,indir}$	$E_{g,dir}$	$E_{g,indir}$
α-HgS	1.250	1.219	1.250	1.209	2.152	2.106
$SnPb_2O_4$	2.195	2.087	2.195	2.088	3.257	3.168
Tetragonal Pb_3O_4	1.173	1.095	1.173	1.095	2.047	1.985

Table 3 Calculated direct and indirect energy gaps ($E_{g,dir}$/$E_{g,indir}$) from the electronic band dispersions and density of states (DoS) meshes computed at the PBEsol (GGA) level of theory[42], and from DoS meshes calculated at the HSE06 (hybrid) level of theory[44].

Comparing **Figs. 6 (b) and (c)**, it can be seen that LTY and RL have similar valence-band structures, but with differences in the respective conduction bands, leading to substantially different

bandgaps. Despite this, both have direct gaps at Γ, and indirect gaps from M to Γ. The direct and indirect gaps obtained from the band structures and the DoS sampling mesh are very similar, confirming that the energy gaps do indeed occur at (or close to) high-symmetry points in the electronic Brillouin zone.

The presence of direct and indirect transitions with similar energies is consistent with the structure of the transition edges in the reflectance spectra, in that at finite temperature - i.e. when sufficient thermal energy is available for phonon-assisted indirect electronic transitions - one would anticipate seeing multiple electronic absorptions with similar energies. A more detailed analysis of this would require taking into account electron-phonon coupling, which is a challenging undertaking beyond the scope of the present discussion.

Finally, we were not able to obtain satisfactory convergence of band structures calculated with the more accurate HSE06 hybrid functional using the "fake self-consistency" procedure used by VASP. However, to estimate the magnitude of the error in the calculated GGA gaps, we performed single-point HSE06 [44] calculations on the optimised structures and took the bandgaps from the Brillouin-zone sampling mesh. These values are listed alongside the GGA ones in **Table 3**. As expected, the HSE06 gaps are larger than the PBEsol ones, at approx. 2.1 eV (590 nm), 3.2 eV (387 nm) and 2 eV (620 nm) for VRM, LTY and RL, respectively, suggesting that the GGA functional consistently underestimates the gaps by around ~1 eV with respect to the hybrid. The gaps do fall into the same qualitative order, however.

Conclusions

In summary, we have developed a technique for analysing the colour-transition regions of the derivative reflectance spectra of coloured paint films, using a straightforward fitting procedure for devonvoluting the features into a sum of Gaussian peak functions.

The contribution of characteristic peaks from different pigments to the composite transition-edge feature can be used quantitatively to establish the mass fractions of coloured pigments in binary paint mixtures using a calibration curve constructed from a set of reference spectra. Our approach can also potentially be extended to estimate the composition of tints with white pigments, and provides a means to distinguish paint layers (glazes) from homogenous mixtures in some cases.

For several of the systems tested, mixing pigments leads to a blue shifting of the transition-edge features, and in some cases also a change in the relative prominence of edge features, both of which may cause problems for more simplistic analyses, including the widely-used "paint approach" to the Kubelka-Munk theory. Our results also demonstrate that this analysis technique is expected to perform poorly for paint mixtures in which the two components have substantially separated reflectance features, for example red lead and lead-tin yellow.

Electronic-structure calculations indicated the complex structure of the colour-transition features in the pigments analysed in this work to be due to shallow band edges and direct and indirect gaps which are close in energy, which give rise to multiple electronic transitions accessible in a narrow energy range.

While proof-of-concept analyses on painted red areas in illuminated medieval manuscripts showed significant promise, more detailed studies need to be done to establish the effects of other variables which were not controlled or examined in the present study, in particular layer thickness, surface texture, pigment particle size, the effects of different paint binders, and the presence of other components likely to be present in real artwork samples, such as varnishes. Overall, however, from

the encouraging results obtained here we expect the analysis technique presented in this work to serve as a valuable tool for the non-invasive analysis of cultural-heritage objects, particularly in conjunction with other well-established techniques such as vibrational spectroscopy.

Acknowledgements

ARP is indebted to St. John's College, Cambridge for providing a scholarship to fund this study, and to ASD Inc. (through the Alexander Goetz programme) and Analytik UK Ltd. for the loan of a Fieldspec 4 spectroradiometer for the completion of this work. JMS is indebted to Trinity College, Cambridge for provision of an Internal Graduate Studentship, and to the UK Engineering and Physical Sciences Research Council (EPSRC) for support under grant no. EP/K004956/1. The computational modelling was performed on the UK national HPC facility (Archer), accessed through the Materials Chemistry Consortium, which is funded through EPSRC grant no. EP/L000202. The authors are also grateful to Dr. Spike Bucklow for valuable discussions which helped to shape this work.

Data-access statement

In addition to the material in the electronic supporting information, the reflectance and derivative-spectra recorded from the model paint samples are available online, free of charge, from [URL to be added on acceptance]. Spectra recorded from artwork samples may be obtained on request from the authors and the Fitzwilliam Museum, Cambridge. The online repository also contains data from the electronic-structure calculations, including the optimised structures.

References

[1] S.P. Best, R.J.H. Clark, R. Withnall, Endeavour, 16 (1992) 66-73.
[2] L. Burgio, R.J.H. Clark, Spectrochimica Acta Part A: Molecular and Biomolecular Spectroscopy, 57 (2001) 1491-1521.
[3] K. Castro, M. Perez-Alonso, M.D. Rodriguez-Laso, L.A. Fernandez, J.M. Madariaga, Analytical and Bioanalytical Chemistry, 382 (2005) 248-258.
[4] F. Rosi, A. Federici, B.G. Brunetti, A. Sgamellotti, S. Clementi, C. Miliani, Analytical and Bioanalytical Chemistry, 399 (2011) 3133-3145.
[5] N. Salvado, S. Buti, E. Pantos, F. Bahrami, A. Labrador, T. Pradell, Applied Physics A: Materials Science & Processing, 90 (2008) 67-73.
[6] L. Appolonia, D. Vaudan, V. Chatel, M. Aceto, P. Mirti, Analytical and Bioanalytical Chemistry, 395 (2009) 2005-2013.
[7] J. Romero-Pastor, C. Cardell, E. Manzano, A. Yebra-Rodriguez, N. Navas, Journal of Raman Spectroscopy, 42 (2011) 2137-2142.
[8] A. Pallipurath, R.V. Vofely, J. Skelton, P. Ricciardi, S. Bucklow, S. Elliott, Journal of Raman Spectroscopy, 45 (2014) 1272-1278.
[9] A. Pallipurath, J. Skelton, S. Bucklow, S. Elliotta, Talanta, 144 (2015) 977–985.
[10] M. Bacci, M. Picollo, G. Trumpy, M. Tsukada, D. Kunzelman, Journal of the American Institute for Conservation, 46 (2007) 27-37.
[11] G. Dupuis, M. Elias, L. Simonot, Applied Spectroscopy, 56 (2002) 1329-1336.

[12] P. Ricciardi, J.K. Delaney, M. Facini, J.G. Zeibel, M. Picollo, S. Lomax, M. Loew, Angewandte Chemie International Edition, 51 (2012) 5607-5610.
[13] P. Ricciardi, J.K. Delaney, M. Facini, L. Glinsman, Journal of the American Institute for Conservation, 52 (2013) 13-29.
[14] C. Colombo, S. Bracci, C. Conti, M. Greco, M. Realini, X-Ray Spectrometry, 40 (2011) 273-279.
[15] L. Burgio, R.J.H. Clark, K. Theodoraki, Spectrochimica Acta Part A: Molecular and Biomolecular Spectroscopy, 59 (2003) 2371-2389.
[16] G. Dupuis, M. Menu, Applied Physics A: Materials Science & Processing, 83 (2006) 469-474.
[17] I.G. Goncalves, C.O. Petter, J.L. Machado, Clays and Clay Minerals, 60 (2012) 473-483.
[18] D. Lehr, M. Luka, M.R. Wagner, M. Bulger, A. Hoffmann, S. Polarz, Chemistry of Materials, 24 (2012) 1771-1778.
[19] M. Doi, R. Ohtsuki, S. Tominaga, Proceedings of the 14th Scandanavian Conference on Image Analysis, 3540 (2005) 95-104.
[20] C. Calvo, Revista Espanola De Ciencia Y Tecnologia De Alimentos, 33 (1993) 597-605.
[21] D.J. McClements, W. Chantrapornchai, F. Clydesdale, Journal of Food Science, 63 (1998) 935-939.
[22] R.S. Berns, M. Mohammadi, Color Research and Application, 32 (2007) 201-207.
[23] G. Dupuis, M. Menu, Applied Physics A: Materials Science & Processing, 80 (2005) 667-673.
[24] J.M.F. Rodriguez, J.A.F. Fernandez, Color Research and Application, 30 (2005) 448-456.
[25] F.R. Stauffer, H. Sakai, Applied Optics, 7 (1968) 61-65.
[26] H. Mark, J. Workman, Spectroscopy, 18 (2003) 32-37.
[27] H. Mark, J. Workman, Spectroscopy, 18 (2003) 25-28.
[28] H. Mark, J. Workman, Spectroscopy, 18 (2003) 106-111.
[29] A.S. Nateri, E. Ekrami, Color Research and Application, 35 (2010) 193-199.
[30] P. Binski, S. Panayotova (Eds.), The Cambridge Illuminations. Ten Centuries of Book Production in the Medieval West, Harvey Miller/Brepols, 2005.
[31] Python Software Foundation, https://www.python.org.
[32] http://www.numpy.org.
[33] E. Jones, T. Oliphant, P. Peterson and others, SciPy: Open source scientific tools for Python, 2001, http://www.scipy.org.
[34] R.H. Byrd, P. Lu, J. Nocedal, C. Zhu, SIAM Journal on Scientific Computing, 16 (1995) 1190-1208.
[35] C. Zhu, R.H. Byrd, P. Lu, J. Nocedal, ACM Transactions on Mathematical Software, 23 (1997) 550-560.
[36] S.T. Gross, Journal of the American Chemical Society, 65 (1943) 1107-1110.
[37] H. Buckley, W. Vernon, Mineralogical Magazine, 20 (1925) 382-392.
[38] J.R. Gavarri, J.P. Vigouroux, G. Calvarin, A.W. Hewat, Journal of Solid State Chemistry, 36 (1981) 81-90.
[39] G.A. Bordovskii, N.L. Gordeev, A.N. Ermoshkin, V.A. Izvozchikov, R.A. Evarestov, Physica Status Solidi: Basic Research, 115 (1983) K15-K19.
[40] H.J. Terpstra, R.A. DeGroot, C. Haas, Journal of Physics and Chemistry of Solids, 58 (1997) 561-566.
[41] B. Hapke, Journal of Geophysical Research, 86 (1981) 3039-3054.
[42] J.P. Perdew, A. Ruzsinszky, G.I. Csonka, O.A. Vydrov, G.E. Scuseria, L.A. Constantin, X.L. Zhou, K. Burke, Physical Review Letters, 100 (2008), 136406.
[43] K. Momma, F. Izumi, Journal of Applied Crystallography, 44 (2011) 1272-1276.
[44] A.V. Krukau, O.A. Vydrov, A.F. Izmaylov, G.E. Scuseria, The Journal of Chemical Physics, 125 (2006), 224106.